Article citation info:
Xiang S., Wang Y., Zhao J. 2026. Microscopic Damage Mechanism of Chinese Fir Subjected to Environmental Aging Consisting of Ultraviolet Irradiation, Thermal-Humidity Cycling, and Salt Fog. *Drewno. Prace naukowe. Doniesienia. Komunikaty.* https://doi.org/10.53502/wood-213884

Łukasiewicz Poznań Institute of Technology

Drewno. Prace naukowe. Doniesienia. Komunikaty
Wood. Research papers. Reports. Announcements

Journal website: https://drewno-wood.pl

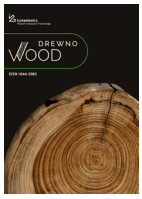

Microscopic Damage Mechanism of Chinese Fir Subjected to Environmental Aging Consisting of Ultraviolet Irradiation, Thermal-Humidity Cycling, and Salt Fog

ShiJie Xiang[a *]
YaChao Wang[a, b, c]
JiangPing Zhao[a]

[a] School of Resources Engineering, Xi'an University of Architecture & Technology, Xi'an, Shaanxi 710055, China
[b] State Key Laboratory of Tropic Ocean Engineering Materials and Materials Evaluation, Hainan University, Haikou 570228, China
[c] State Key Laboratory of Safety and Resilience of Civil Engineering in Mountain Area, East China Jiao Tong University, Nanchang 330013, China

Article info
Received: 19 August 2025
Accepted: 3 November 2025
Published: 12 January 2026

Keywords
Chinese fir
accelerated aging
environmental factors
mechanical properties
microstructure

This study comparatively investigates the degradation of Chinese fir under three accelerated aging protocols simulating key environmental threats: ultraviolet (UV) weathering, thermal-humidity cycling, and salt fog. The results revealed distinct degradation mechanisms with significant implications for heritage diagnostics. Salt fog exposure induced the most severe degradation, causing a 63.9% loss in bending strength through comprehensive chemical attacks. UV weathering led to significant surface photodegradation and microcracking, while thermal-humidity cycling caused a 46.5% reduction in bending strength, primarily due to physical stresses. Crucially, a strong, universal correlation was established between cellulose crystallinity (CrI) and the mechanical properties (tensile, R=0.874; compressive, R=0.902; bending, R=0.941) across all aging conditions. This identifies CrI as a robust and minimally invasive indicator for assessing the mechanical integrity of historic timbers. Furthermore, the degradation kinetics under each stressor followed highly predictable trends, with UV weathering and thermal-humidity cycling exhibiting strong linear relationships (R^2>0.96), and salt fog also showing a clear linear trend (R^2>0.84). This provides a quantitative basis for developing targeted conservation strategies and more accurate service life prediction models for timber heritage structures.

DOI: 10.53502/wood-213884

Introduction

Chinese fir (*Cunninghamia lanceolata*) is a cornerstone structural material in traditional Chinese architecture, prized for its favorable mechanical properties and natural durability [1]. For centuries, it has been the primary timber for constructing iconic heritage structures, making the preservation of its long-term performance a cultural imperative as well as an engineering challenge [2],[4]. However, these historic structures are constantly exposed to harsh environmental stressors, including intense solar radiation, drastic hygrothermal fluctuations, and saline air in coastal regions, which can cause substantial degradation in mechanical strength [5]. Despite its importance, the specific mechanisms governing its degradation under these distinct conditions remain poorly understood. This knowledge gap presents a critical barrier to developing effective service-life prediction models and targeted conservation strategies for irreplaceable timber heritage [6],[7].

Existing research has typically investigated the effects of individual environmental factors in isolation.

* Corresponding author: x1151658268@xauat.edu.cn

For instance, ultraviolet (UV) radiation is known to trigger the photodegradation of lignin [8], while hygrothermal cycling induces internal stresses that cause micro-cracking [9],[10]. Concurrently, chemical agents, such as those in saline environments, can accelerate the hydrolysis of structural polymers [11],[12]. While these studies provide valuable insights into specific damage modes, their isolated approach fails to capture the complex interplay and, critically, the comparative severity of these factors as experienced by heritage structures. Consequently, how these distinct environmental threats uniquely impact the material's integrity remains largely unquantified.

This landscape reveals critical gaps in conservation science. First, without a comparative benchmark, it is difficult to perform accurate in-situ diagnosis of deterioration causes in historic buildings, as each stressor may leave a unique "damage signature." Second, and more fundamentally, there is a lack of robust quantitative correlations linking micro-level changes (e.g., chemical composition, cellulose crystallinity) to macro-level mechanical performance. Establishing such correlations is essential for developing the minimally invasive or non-destructive assessment techniques that are paramount in heritage conservation [13]–[16]. The absence of this integrated understanding severely hampers both the accurate durability assessment of timber components and the development of targeted preservation strategies [17]–[19].

To address these critical gaps, this study systematically investigates the degradation of Chinese fir under three distinct accelerated aging protocols: UV weathering, hygrothermal cycling, and salt fog exposure. By integrating mechanical testing with comprehensive microstructural and chemical analyses (SEM, XRD, FTIR), this work aims to: (1) comparatively elucidate the unique damage mechanisms and severity driven by each environmental stressor, establishing their distinct "damage signatures"; and (2) establish universal, quantitative correlations between a key microstructural indicator—cellulose crystallinity—and the resulting loss of mechanical strength. The findings are intended to provide a robust scientific framework for the assessment, conservation, and management of Chinese fir in architectural heritage.

Materials and methods

1. Specimen Preparation

Clear, defect-free Chinese fir (*Cunninghamia lanceolata*) lumber was sourced from an approximately 30-year-old sustainable plantation in Fujian Province, China. The lumber was conditioned at 20±2°C and 65±5% relative humidity (RH) to a constant mass, achieving an equilibrium moisture content (EMC) of approximately 12% and an average air-dry density of 380 kg/m^3. Subsequently, the lumber was machined into 400 mm (Longitudinal) × 200 mm (Tangential) × 10 mm (Radial) blocks. Each block was then quarter-sawn to yield four matched sub-specimens (100mm× 100mm× 10mm). For a robust comparative analysis, one specimen from each matched set was designated as the unaged control, while the other three were allocated to the UV weathering, thermal-humidity cycling, and salt fog exposure protocols, respectively.

2. Accelerated Aging Protocols

Three distinct accelerated aging protocols were employed to simulate long-term environmental exposure, with the key parameters for each summarized in Table 1. The parameters for each accelerated aging protocol were carefully selected based on several key principles to ensure scientific rigor and relevance. Firstly, the protocols adhere strictly to established international standards to guarantee the reproducibility and comparability of the results. Secondly, the conditions were chosen to simulate the typical and often harsh environmental stressors faced by historic timber structures in China, such as intense summer solar radiation, severe temperature fluctuations in continental climates, and corrosive saline air in

Table 1. Summary of accelerated aging protocols

Aging Protocol	Abbreviation	Aging Durations (days)	Key Parameters	Standard
Unaged	Unaged	0	Stored at 20 ± 2 °C, 65 ± 5% RH	
Thermal-Humidity Cycling	THC	3, 7, 14, 30	Cycle: 70 °C → 25 °C (95% RH) → -40 °C→ 25 °C (95% RH)	IEC 60068-2-30
UV Weathering	UV	3, 7, 14, 30	Cycle: 8h UVA (0.76 W/m², 60°C BPT) + 4h dark/spray (50°C BPT)	ISO 4892-3
Salt Fog Exposure	SF	3, 7, 14, 30	Cycle: 12h spray (5% NaCl, 22.4°C, pH 6.5–7.2) + 12h rest	ISO 9227

coastal regions. Finally, the parameters were informed by existing literature on wood degradation to ensure the accelerated aging was both effective and representative of natural degradation processes.

For Thermal-Humidity Cycling (THC), the protocol was based on IEC 60068-2-30:2005 [20]. The upper temperature of 70°C simulates the peak surface temperature of wood under direct summer sun, while the lower temperature of -40°C represents extreme winter conditions found in northern China. The high humidity level (95% RH) simulates damp climatic conditions, and the drastic cycling between these states is highly effective at inducing internal physical stresses.

For UV Weathering, the conditions followed ISO 4892-3:2016 [21]. The irradiance of 0.76 W/(m²·nm) at 340 nm and a black-panel temperature of 60°C are standard accelerated conditions designed to mimic intense sunlight, focusing on the UVA spectrum, which is particularly damaging to lignin in wood.

For Salt Fog (SF) Exposure, the test was conducted according to ISO 9227:2022 [22]. A 5% NaCl solution is the standard concentration used to simulate a marine atmosphere, widely employed to assess the durability of materials in coastal environments.

2.1. Thermal-Humidity Cycling

Thermal-humidity cycling was conducted in a programmable environmental chamber (BPHJS-060A) following the IEC 60068-2-30:2005 standard [20]. Each 24-hour cycle consisted of four sequential steps: (1) ramping to 70±2s°C over 2 h and holding for 4 h (humidity uncontrolled); (2) cooling to 25±3°C over 2 h and holding for 4 h at 95±3% RH; (3) cooling further to −40±3°C over 2 h and holding for 4 h (humidity uncontrolled); and (4) ramping back to 25±3°C over 2 h and holding for 4 h at 95±3% RH. This cycle was repeated continuously for total durations of 3, 7, 14, and 30 days.

2.2. UV Weathering

UV weathering was performed in a UV chamber (Model: FR-120S) according to the ISO 4892-3:2016 standard [21]. A complete 12-hour cycle consisted of an 8 h exposure to UVA-340 lamps at an irradiance of 0.76 W/(m² · nm) (at 340 nm) and a blackboard temperature (BPT) of 60±3°C. This was followed by a 4 h dark phase comprising 0.25 h of water spray and 3.75 h of condensation at a BPT of 50±3°C. The entire cycle was repeated continuously for the specified durations.

2.3. Salt Fog Exposure

A neutral salt spray test was conducted in a salt fog chamber (Model: FR-90) per the ISO 9227:2022 standard to simulate a corrosive environment [22]. The protocol involved a 24-hour cycle: 12h of continuous spraying with a 5% NaCl solution, followed by 12 h of rest in a saturated humidity environment. The chamber temperature was maintained at 22.4±2°C, and the pH of the salt solution was controlled between 6.5 and 7.2. This cycle was repeated for the specified durations.

Aging of Chinese fir specimens is conducted according to the aging process depicted in **Fig. 1**, where SF represents salt fog exposure, UV denotes ultraviolet aging, and THC signifies thermal-humidity cycling aging.

3. Characterization and Mechanical Testing

3.1. Microstructural and Chemical Analysis

Scanning Electron Microscopy (SEM): Surface morphology and cross-sectional microstructures were examined using a scanning electron microscope (FEI Quanta 250). Samples (12mm radial× 2.5mm tangential× 2mm longitudinal) were cut from both aged and control specimens and sputter-coated with

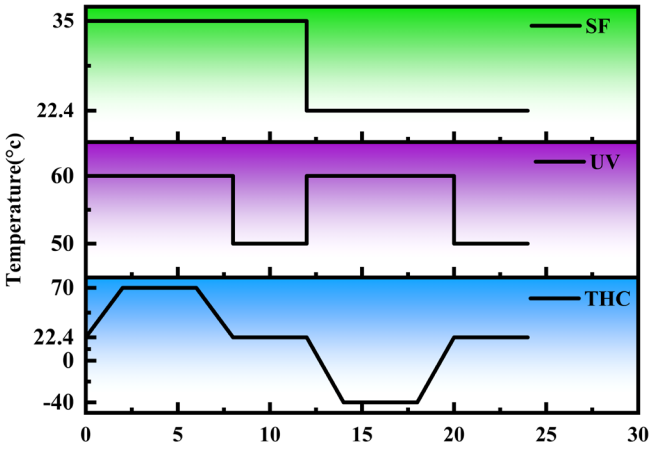

Fig. 1. Temperature profiles for the three accelerated aging protocols: thermal-humidity cycling (THC), UV weathering (UV), and salt fog exposure (SF)

a thin gold layer before imaging to ensure electrical conductivity.

Fourier-Transform Infrared (FTIR) Spectroscopy: Changes in chemical functional groups were analyzed with an FTIR spectrometer (Nexus 670). Wood shavings from specimen surfaces were mixed with potassium bromide (KBr) powder (mass ratio approx. 1:150) and pressed into translucent pellets. Spectra were recorded from 4000 to 400 cm^{-1} at a resolution of 4 cm^{-1}, averaging 16 scans per sample.

X-ray Diffraction (XRD): The effect of aging on cellulose crystallinity was investigated using an X-ray diffractometer (MiniFlex 600) with a Cu Kα radiation source (λ=0.154nm). Dried, ground wood powder was scanned over a 2θ range of 5◦ to 50◦ at a rate of 2◦/min. The cellulose crystallinity index (CrI) was calculated using the Segal method [23]:

$$X_c = \frac{I_{002} - I_{am}}{I_{002}} \times 100\% \quad (1)$$

Where I_{002} is the maximum intensity of the (002) lattice diffraction peak (at 2θ ≈ 22.5°) and I_{am} is the intensity of diffraction of the amorphous background (at 2θ ≈ 18°).

3.2. Physical Property Analysis

Colorimetry: Surface color changes are quantified using a color difference analyzer (LS170). The color is characterized in the CIE L*a*b* color space, where L* represents lightness, a* represents the red-green axis, and b* represents the yellow-blue axis. The total color difference (ΔE*) relative to the unaged control is calculated using Eq. (2)

$$\Delta E^* = \left[(\Delta L^*)^2 + (\Delta a^*)^2 + (\Delta b^*)^2 \right]^{1/2} \quad (2)$$

3.3. Mechanical Property Testing

All mechanical tests are performed using a universal testing machine (WE-30) under ambient laboratory conditions.

Tensile Strength: Longitudinal tensile strength is evaluated according to ISO 13061-6:2014 [24]. Specimens are loaded at a constant displacement rate of 2 mm/min until failure.

Compressive Strength: Longitudinal compressive strength is determined following ISO 13061-17:2017. A loading rate of 2 mm/min is applied until failure [25].

Bending Strength and Modulus of Elasticity (MOE): Three-point bending tests are conducted based on ISO 13061-3:2014 (bending strength) and ISO 13061-4:2014 (MOE) [26],[27]. The specimens are placed on two supports with a span of 240 mm. For MOE determination, the specimen is first loaded to approximately 40% of its predicted failure load at a rate of 1 mm/min while recording the deflection. Subsequently, the loading rate is increased to 3 mm/min until fracture to determine the bending strength.

Results and analysis

1. Mechanical Property Degradation

The effects of the three accelerated aging protocols on the mechanical properties of Chinese fir were systematically evaluated. Significant degradation was observed across all measured properties—tensile, compressive, and bending strength—with the extent and nature of the loss varying distinctly with the type of environmental stressor.

1.1. Longitudinal Tensile Strength

The effects of the three accelerated aging protocols on the longitudinal tensile strength of Chinese fir are presented in Fig. 2 and Table 2.

The unaged control specimens exhibit an average tensile strength of 77.19 MPa. Following all aging treatments, a consistent decline in tensile strength is observed, with the extent of degradation varying significantly among the different protocols.

Based on the test results, the longitudinal tensile strength of the specimens is calculated using Eq. (3):

$$\sigma_{TW} = \frac{P_{max}}{tb} \quad (3)$$

In the equation, σ_{tw} represents the longitudinal tensile strength at a moisture content of W, with units in MPa; P_{max} is the failure load in N; b is the specimen width in mm; and t is the specimen thickness in mm.

Salt fog exposure induces the most substantial loss of tensile strength. The strength decreases progressively, reaching a final value of 32.94 MPa after 30 days, which corresponds to a 57.4% reduction. This severe degradation suggests a pervasive chemical attack on the wood's primary load-bearing components [28],[29].

UV weathering also leads to a significant, albeit lesser, reduction in tensile strength. After 30 days of exposure, the strength drops to 57.63 MPa (a 25.3% reduction). This degradation is mainly attributed to the photodegradation of lignin at the surface, which creates microcracks that compromise the material's structural integrity [30].

Thermal-humidity cycling causes a moderate but steady decline in tensile strength. The strength

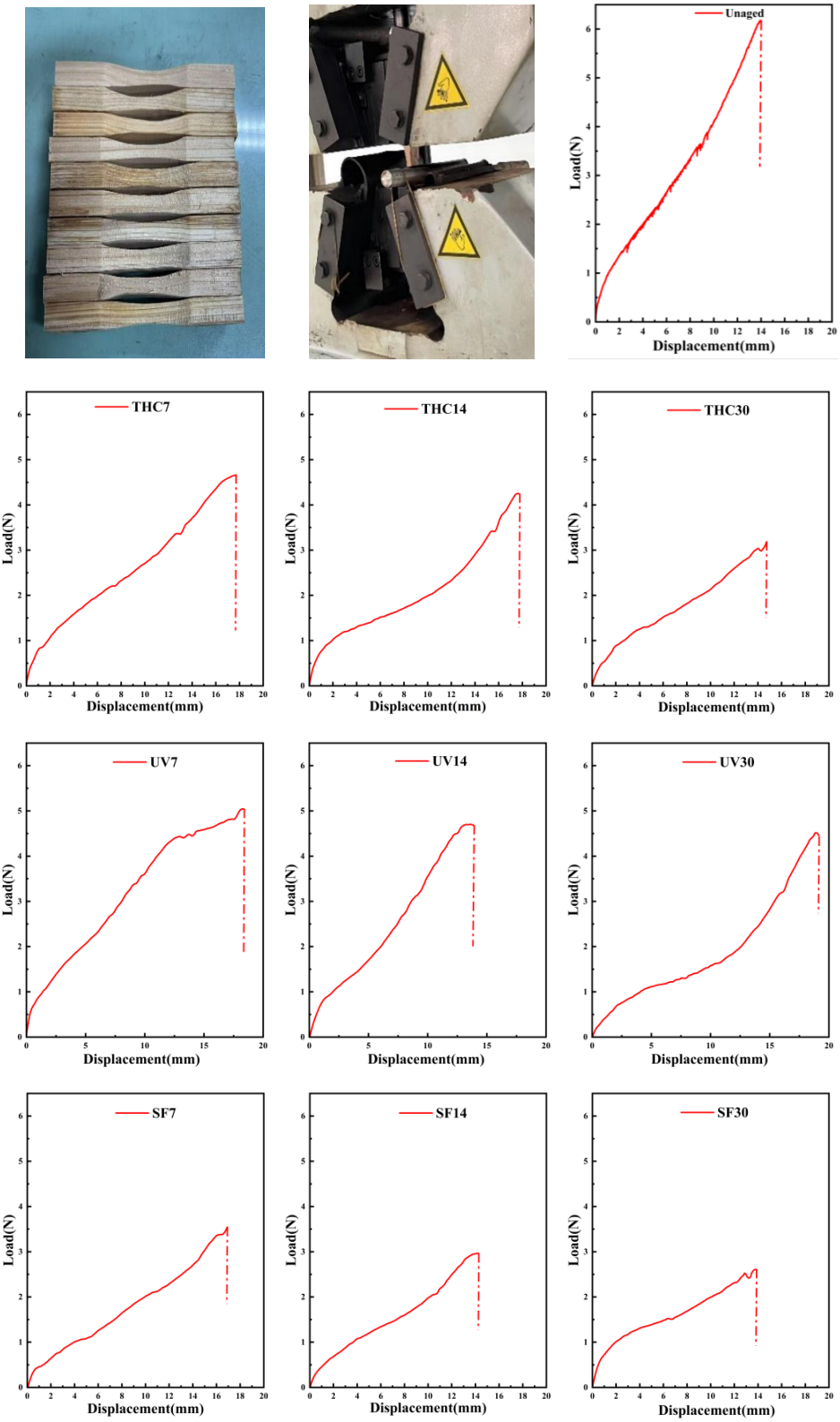

Fig. 2. Longitudinal Tensile Specimens and Test Images

reduces by 43.9% over the 30 days. This effect is primarily mechanical in nature, arising from internal stresses generated by the anisotropic expansion and contraction of wood components during temperature and moisture fluctuations.

In summary, the hierarchy of degradation severity for tensile strength is as follows: Salt Fog > Thermal-Humidity Cycling > UV Weathering.

Table 2. Key Data for Longitudinal Tensile Strength

	Unaged	UV7	UV14	UV30	THC7	THC14	THC30	SF7	SF14	SF30
Maximum Force (N)	6174.7	5058.0	4719.9	4610.1	4663.8	4330.8	3152.7	3537.0	2970.9	2635.5
Tensile Strength (MPa)	77.19	63.23	59.00	57.63	58.30	54.14	39.41	44.21	37.14	32.94

Note: Aging conditions are denoted as: UV (ultraviolet weathering), THC (thermal-humidity cycling), and SF (salt fog exposure).
The number following the abbreviation indicates the aging duration in days (e.g., THC14 represents 14 days of thermal-humidity cycling)

1.2. Longitudinal Compressive Strength

The degradation trends for longitudinal compressive strength under the three aging protocols are illustrated in Fig. 3 and detailed in Table 3. The compressive strength of Chinese fir shows a consistent decrease following all aging treatments, exhibiting a pattern analogous to that observed for tensile strength. The unaged control specimens possess an average compressive strength of 68.97 MPa.

Based on the test results, the longitudinal compressive strength is calculated using Equation (4):

$$\sigma_{cw} = \frac{P_{max}}{bt} \tag{4}$$

In the equation, σ_{cw} represents the longitudinal compressive strength, with units in MPa; P_{max} is the failure load in N; t is the specimen thickness in mm; and b is the specimen width in mm.

Again, salt fog exposure induces the most pronounced degradation. The compressive strength declines by 49.1% after 30 days, reaching a final value of 35.14 MPa. This substantial loss is linked to the deep-level chemical degradation of the cell wall matrix, particularly the disruption of the rigid lignin network, which is a key contributor to compressive strength [31].

UV weathering results in a more moderate reduction, with a decrease of 31.6% over the 30 days. The impact of UV radiation on compressive strength is less severe than on tensile strength, suggesting that surface-level photodegradation of lignin has a comparatively smaller effect on the bulk properties governing compression resistance [32].

Thermal-humidity cycling leads to a strength reduction of 34.8% after 30 days. The magnitude of this reduction is comparable to that caused by UV aging, indicating that physical damage, such as micro-cracking from internal stresses, also plays a significant role in compromising the wood's ability to resist compressive loads.

Overall, the hierarchy of degradation severity for compressive strength follows the same order as that for tensile strength: Salt Fog > Thermal-Humidity Cycling ≈ UV Weathering.

1.3. Bending Strength and Modulus of Elasticity (MOE)

The results of the three-point bending tests, which assess both bending strength (Modulus of Rupture, MOR) and Modulus of Elasticity (MOE), are presented in Fig. 4 and Table 4. These properties are critical for evaluating the structural performance of timber beams. The unaged Chinese fir specimens possess a bending strength of 59.62 MPa and an MOE of 11.45 GPa.

Table 3. Key Data for Compressive Strength

	Unaged	UV7	UV14	UV30	THC7	THC14	THC30	SF7	SF14	SF30
Maximum Force (N)	6896.56	6642.62	5462.62	4720.36	5558.76	4604.88	4498.38	5335.44	4591.48	3514.44
Compressive Strength (MPa)	68.97	66.43	54.63	47.20	55.59	46.05	44.98	53.35	45.92	35.14

Note: Aging conditions are denoted as: UV (ultraviolet weathering), THC (thermal-humidity cycling), and SF (salt fog exposure).
The number following the abbreviation indicates the aging duration in days (e.g., THC14 represents 14 days of thermal-humidity cycling)

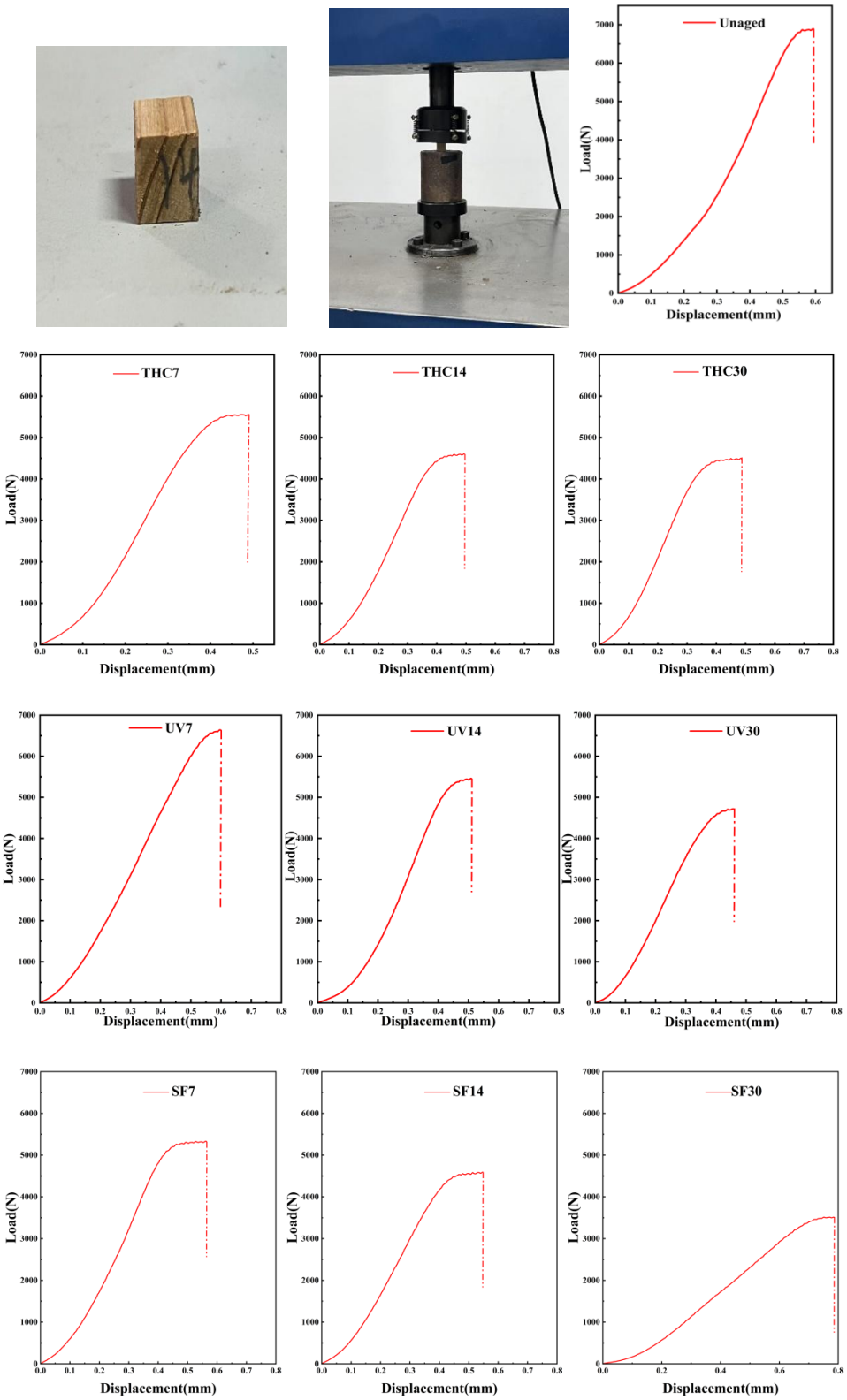

Fig. 3. Longitudinal Compressive Specimens and Test Images

After all specimens are tested, the bending elastic modulus and bending strength of the specimens are calculated using Equations (5) and (6):

$$E = \frac{FL^3}{4bh^3\delta} \tag{5}$$

In the equations, E represents the elastic modulus with units in GPa; L is the span between two supports in mm; b is the specimen width in mm; h is the specimen height in mm; and δ is the deflection at the midpoint of the specimen in mm.

$$\sigma_b = \frac{3F_{max}L}{2bh^2} \quad (6)$$

In the equations, σ_b represents the bending strength of the specimen in MPa; F_{max} is the peak load at specimen fracture in N; L is the span between two supports in mm; b is the specimen width in mm; and h is the specimen height in mm.

Consistent with the tensile and compressive tests, salt fog exposure exerts the most detrimental effect. The bending strength decreases dramatically by 63.9% after 30 days. The MOE also shows a significant decline,

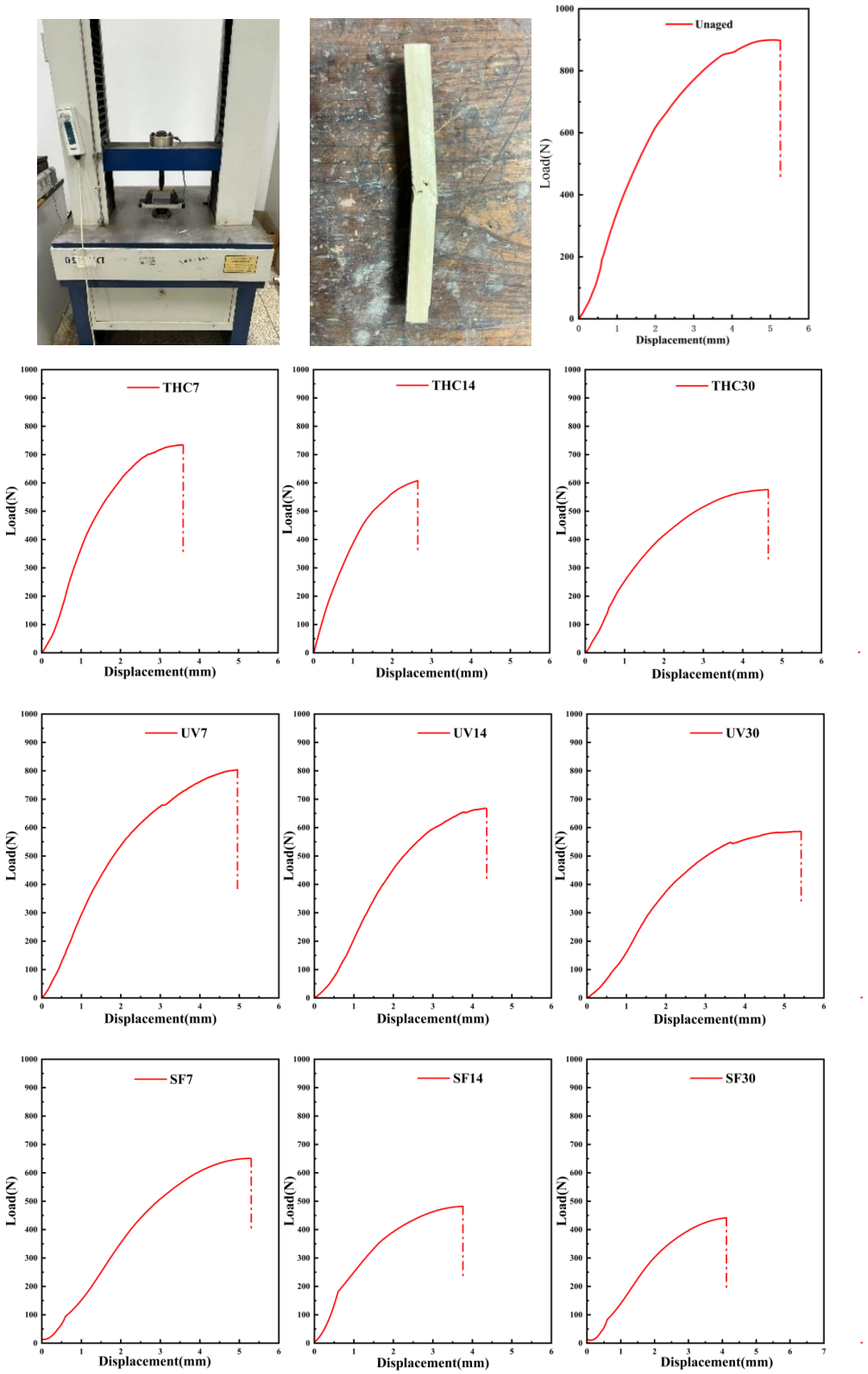

Fig. 4. Bending Specimens and Test Images

Table 4. Key Data for Three-Point Bending

	Unaged	UV7	UV14	UV30	THC7	THC14	THC30	SF7	SF14	SF30
Elastic Modulus (GPa)	11.45	10.95	10.25	8.57	10.86	8.86	7.58	9.85	6.67	5.85
Bending Strength (MPa)	59.62	55.18	52.35	35.02	53.57	43.39	31.90	49.41	27.96	21.51

Note: Aging conditions are denoted as: UV (ultraviolet weathering), THC (thermal-humidity cycling), and SF (salt fog exposure). The number following the abbreviation indicates the aging duration in days (e.g., THC14 represents 14 days of thermal-humidity cycling)

Table 5. Surface Color Values of Chinese Fir Before and After Aging Treatment

		L*		a*		b*		h		ΔE*	
Sample	T (d)	Mean	SD	Mean	SD	Mean	SD	Mean	SD	Mean	SD
Unaged	0	70.74	3.71	10.11	0.74	45.73	0.93	77.50	0	0	0
UV	3	60.18	9.71	14.54	1.12	38.67	1.34	69.38	0.97	13.54	1.31
	7	54.19	11.31	16.48	1.24	37.93	0.92	66.51	1.17	19.37	1.22
	14	41.40	10.73	16.90	1.23	34.89	1.39	64.15	1.89	32.01	0.98
	30	37.89	12.49	29.17	1.09	27.02	1.93	63.37	1.44	42.34	1.37
THC	3	66.99	9.27	11.46	1.17	32.84	1.07	70.76	1.19	13.49	0.89
	7	60.01	11.92	12.71	1.05	32.58	1.42	68.68	1.52	17.17	1.12
	14	55.37	8.39	18.60	1.32	32.02	1.78	59.84	1.73	22.28	0.93
	30	44.76	12.94	18.56	1.41	30.21	1.59	58.48	1.29	31.42	1.39
SF	3	69.97	9.78	9.31	1.29	37.89	1.82	76.18	1.03	7.92	0.83
	7	63.50	10.21	11.37	1.17	39.83	1.14	74.04	1.38	9.42	1.02
	14	59.96	11.43	14.05	1.33	34.08	1.67	67.58	0.91	16.35	0.96
	30	58.56	9.97	12.84	1.41	29.22	1.32	66.28	1.47	20.70	1.19

Note: Aging conditions are denoted as UV (ultraviolet weathering), THC (thermal-humidity cycling), and SF (salt fog exposure). The number following T(d) indicates the aging duration in days

underscoring the comprehensive damage to the cell wall structure that affects both its ultimate load capacity and its elastic response.

Thermal-humidity cycling induces substantial reductions in bending properties, with bending strength decreasing by 46.5% over the 30 days. The MOE follows a similar downward trend. This indicates that the physical stresses from thermal cycling effectively disrupt the integrity of the wood matrix.

Among the three protocols, UV weathering causes the most gradual decline in bending strength, with a reduction of 41.3% at the 30-day mark. The impact on MOE is also the least pronounced. This finding suggests that the surface-focused degradation from UV radiation has a less immediate impact on bending properties, which are more dependent on the bulk integrity of the entire cross-section [33].

2. Surface Color Alteration

The surface color changes of Chinese fir under the different aging protocols are quantified using the CIE Lab* colorimetric system, with the detailed parameter changes presented in Fig. 5 and Table 5. The overall degradation kinetics, represented by the total color difference (ΔE*), were further analyzed to assess their predictability. As shown in Fig. 6, the color difference under all three protocols exhibited a highly predictable linear relationship with aging time. Specifically, UV weathering and thermal-humidity cycling showed strong linear correlations ($R^2_{Adj} > 0.96$), and salt fog also followed a clear linear trend ($R^2_{Adj} = 0.844$). This indicates that the color degradation process proceeds at a nearly constant rate under these accelerated conditions. This predictability is fundamental for

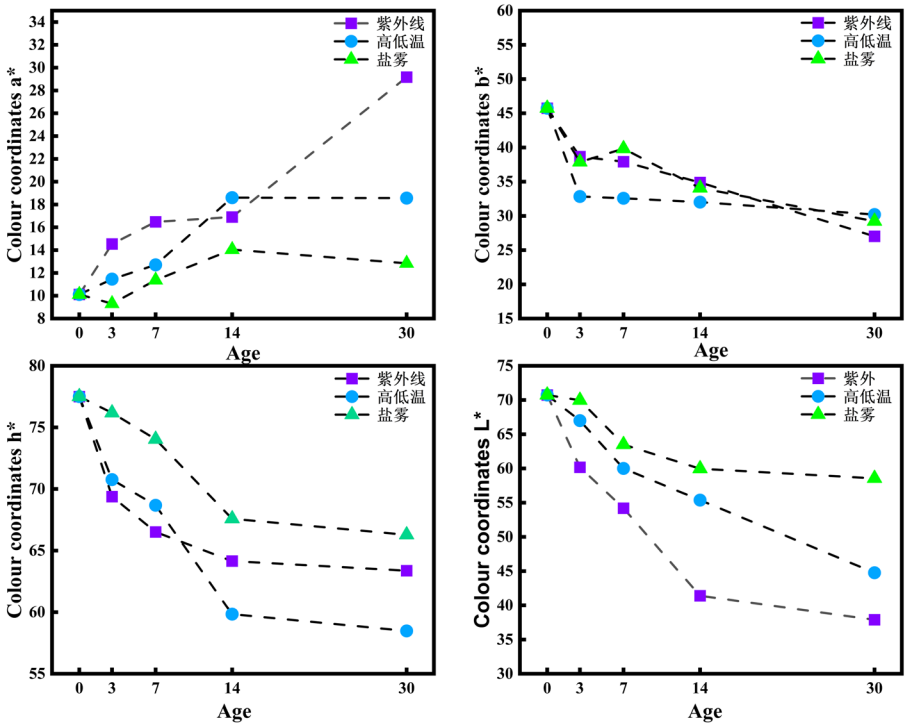

Fig. 5. Color Changes of Unaged and Three Differently Aged Chinese Fir

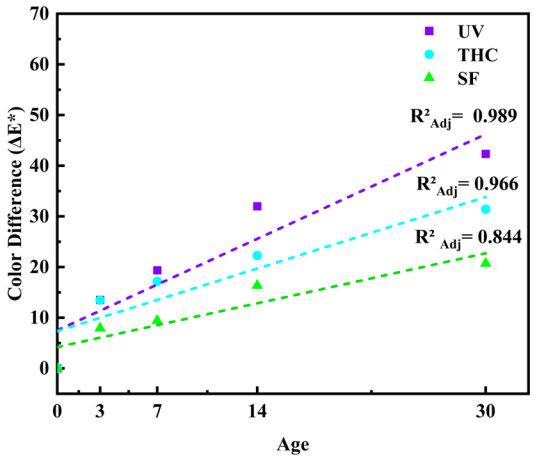

Fig. 6. Linear regression analysis of color difference (ΔE*) as a function of aging time for Chinese fir under different aging protocols

developing service-life prediction models for timber heritage structures.

UV weathering induces the most dramatic and rapid color changes. The lightness (L*) value decreases sharply from an initial 70.74 to 37.89 after 30 days, indicating significant surface darkening. Concurrently, the red-green chromaticity index (a*) increases, signifying a shift towards red, while the yellow-blue index (b*) decreases, indicating a shift towards blue. These combined changes result in a substantial total color difference (ΔE*) of 42.34. This phenomenon is attributed to the photodegradation of lignin, wherein UV energy promotes oxidation reactions that form chromophoric (color-bearing) quinone-like structures and other red-shifted compounds [34]. The formation of a darkened, carbonized surface layer also masks the wood's original yellow hue, contributing to the observed changes [35].

Thermal-humidity cycling causes a moderate and more gradual alteration of the wood's color. The L* value shows a steady decline, leading to a final ΔE* of 31.42. This change is likely driven by physical mechanisms, such as surface micro-roughening and the redistribution of pigment substances induced by hygrothermal stress, rather than extensive chemical reactions [36].

Salt fog exposure results in the least significant color change, with a final ΔE* of only 20.70. While the L* value decreases slightly, the chromaticity coordinates

(a* and b*) remain relatively stable. The primary mechanism appears to be physical soiling and slight surface degradation from the salt solution, which reduces light reflectance but does not induce major chromophoric changes in the wood's chemical components [37],[38].

In summary, the severity of color alteration follows the hierarchy: UV Weathering >> Thermal-Humidity Cycling > Salt Fog. This finding demonstrates that photochemical reactions induced by UV radiation are the dominant driver of color degradation in Chinese fir, far surpassing the effects of physical stress or mild chemical attack.

3. Microstructural, Chemical, and Crystalline Structure Alterations

3.1. Surface Morphology (SEM Analysis)

Scanning electron microscopy (SEM) reveals distinct microstructural changes on the wood surface corresponding to each aging protocol (Fig. 7). Specifically, Fig. 7A shows the surface after 30 days of UV weathering, Fig. 7B after thermal-humidity cycling, and Fig. 7C after salt fog exposure, while Fig. 7D displays the smooth, intact surface of the unaged control specimen.

The unaged control specimen (Fig. 7D) exhibits a smooth and intact surface, with well-ordered and tightly packed wood fibers. In contrast, thermal-humidity cycling induces significant physical damage (Fig. 7B), characterized by prominent cracks and fractures that disrupt fiber continuity, pointing to severe internal stresses [39]. Salt fog exposure leads to severe chemical degradation (Fig. 7C), where cell wall structures appear blurred and partially dissolved, indicating a corrosive attack that penetrates the fiber structure [40]. UV weathering results in a different mode of surface degradation (Fig. 7A), characterized primarily by a network of fine microcracks, a direct consequence of the photochemical degradation of lignin, which weakens intercellular bonding [41].

3.2. Cellulose Crystallinity (XRD Analysis)

The changes in cellulose crystallinity, a key factor influencing wood's mechanical properties, are investigated using X-ray diffraction (XRD), with the results presented in Fig. 8 and Table 6.

Unaged Chinese fir exhibits a cellulose crystallinity index (CrI) of 42.41%. All aging protocols lead to a decrease in CrI, indicating damage to the ordered crystalline regions of cellulose.

Thermal-humidity cycling results in the smallest, yet still significant, decrease in CrI, to a value of 37.36%. This reduction is attributed to physical mechanisms: repeated swelling and shrinking, driven by changes in moisture and temperature, induce mechanical fatigue at the interface between crystalline and amorphous regions, leading to a partial disruption of the crystalline lattice [42].

Salt fog exposure causes the most substantial reduction in crystallinity, with the CrI dropping to 31.88% (a 24.8% relative decrease). This finding is consistent with a chemical degradation pathway wherein the hydrolysis of glycosidic bonds in cellulose and hemicellulose, facilitated by the acidic electrolyte environment, disrupts the ordered molecular chains [43].

UV weathering also reduces crystallinity, resulting in a final CrI of 36.34%. This effect is primarily indirect; the photodegradation of the surrounding lignin matrix weakens its protective function, thereby exposing the cellulose fibrils to degradation. Furthermore, UV radiation can directly cleave cellulose chains, further disrupting the crystalline structure [44], [45].

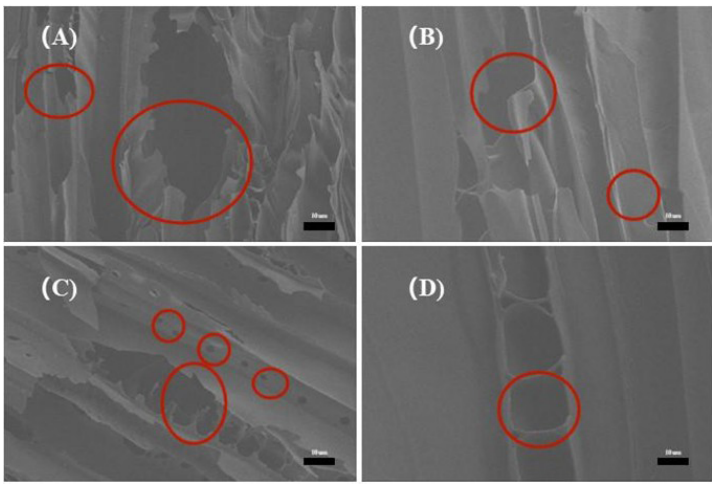

Fig. 7. SEM Images of Unaged and Three Differently Aged Chinese Fir

Table 6. Cellulose Crystallinity of Chinese Fir Samples Under Different Aging Treatments

Sample	Diffraction angle of the (002) crystalline plane of cellulose	Diffraction angle of the (101) crystalline plane of cellulose	Intensity at the (002) crystalline plane (a.u.)	Diffraction peak intensity at a scanning angle close to 16° (a.u.)	Cellulose crystallinity
Unaged	22.04	16.6	349	201	42.41
UV	22.68	16.76	355	224	36.34
THC	22.94	16.06	364	228	37.36
SF	22.4	16.8	389	265	31.88

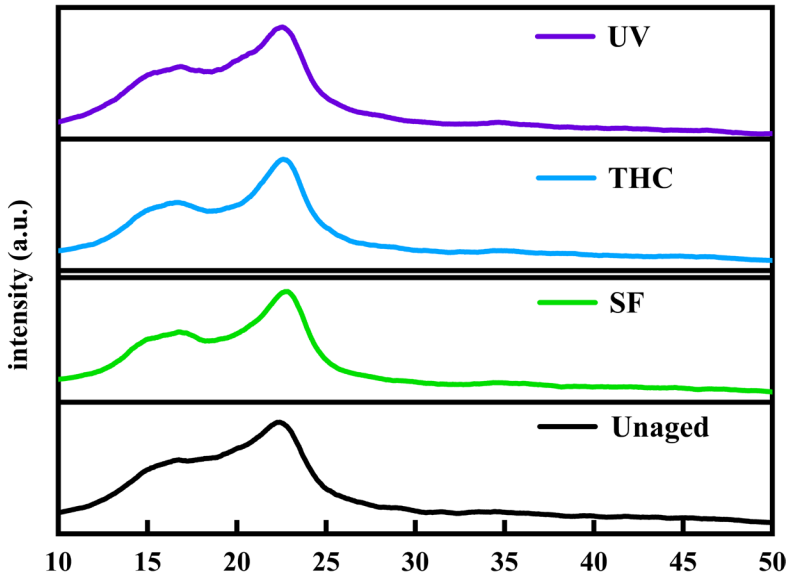

Fig. 8. XRD Diffraction Patterns of Unaged and Three Differently Aged Chinese Fir

3.3. Functional Group Degradation (FTIR Analysis)

FTIR spectroscopy provides insight into the chemical changes in the main components of wood (Fig. 9 and Table 7).

Thermal-humidity cycling shows the most significant impact on the broad hydroxyl (-OH) stretching band at approximately 3350 cm^{-1}, which is characteristic of cellulose. The intensity of this peak decreases notably, suggesting that repeated hygrothermal stresses disrupt the hydrogen bond network within and between cellulose molecules [46],[47]. This physical disruption is a key degradation mechanism under this protocol.

The spectra reveal that salt fog exposure aggressively degrades all major wood polymers. A significant decrease in the intensity of the peak at 1740 cm^{-1} (C=O stretching in hemicellulose) indicates severe hemicellulose degradation. Similarly, pronounced reductions in the peaks at 1508 cm^{-1} (aromatic skeletal vibration) and 1260 cm^{-1} (C-O stretching) point to extensive degradation of the lignin structure [48].

UV weathering primarily targets lignin. This is evidenced by a marked decrease in the characteristic lignin peaks (1508 cm^{-1} and 1260 cm^{-1}), confirming the photochemical breakdown of the aromatic polymer. The impact on cellulose and hemicellulose is less pronounced compared to that of salt fog.

Discussion

1. Distinct Degradation Mechanisms Driven by Environmental Stressors

This study reveals that the three simulated environmental stressors induce fundamentally different degradation pathways in Chinese fir, each leaving a distinct "damage signature" at the macro- and micro-scales.

Salt fog exposure initiated a comprehensive, bulk chemical degradation. The aqueous NaCl solution, acting as a corrosive electrolyte, facilitated the widespread hydrolysis of polysaccharides and the cleavage of lignin's aromatic structure, as confirmed by the broad

Table 7. Changes in Characteristic Peaks

Peak position (cm^{-1})	Characteristic peak description	Decrease under UV aging (%)	Decrease under high-low temperature aging (%)	Decrease under salt fog aging (%)
3350	-OH	18.6	22.4	15.8
2930	$-CH_2-$	14.2	19.5	12.7
1030	C-O-C	12.3	16.8	9.7
1740	C=O	11.5	9.8	17.2
1260	C-O	10.3	13.1	18.4
1508	C_6H_6	13.2	10.7	18.9
1650	C=O	16.8	11.2	19.3

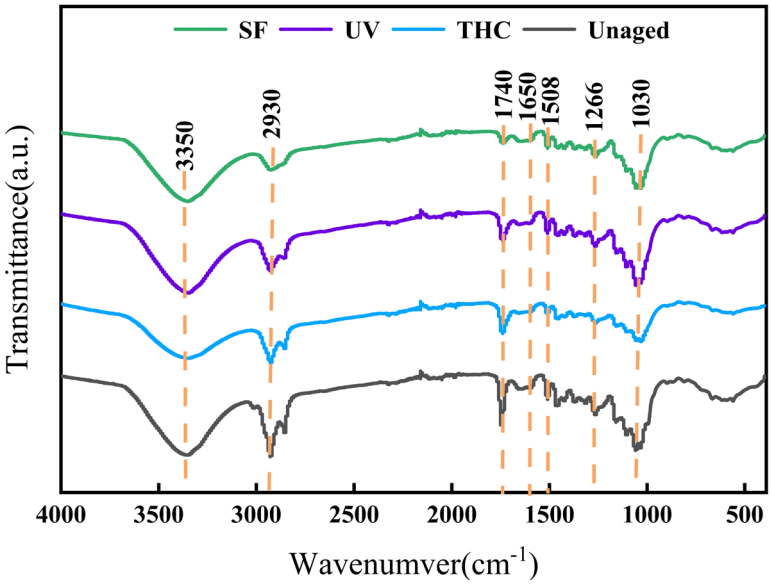

Fig. 9. FT-IR Spectra of Unaged and Three Differently Aged Chinese Fir

functional group degradation in the FTIR analysis [11], [42]. More specifically, the presence of chloride ions (Cl^-) can catalyze the hydrolysis of glycosidic bonds in cellulose and hemicellulose and promote the degradation of lignin's aromatic structure. This deep-level chemical attack provides a direct explanation for the catastrophic and uniform decline across all mechanical properties, which was further evidenced by the severe loss of cellulose crystallinity (a 24.8% relative decrease) and the cellular dissolution observed in SEM images (Fig. 7C).

In stark contrast, UV weathering drove a surface-limited, photochemical degradation. Its primary effect was the breakdown of lignin within the outer micrometers of the wood surface. Lignin's conjugated structures (e.g., aromatic rings, carbonyls) act as the main chromophores that absorb UV radiation, generating free radicals that initiate chain-degradation reactions [49]. This process forms new, colored compounds such as quinone-like structures, which directly explains the drastic color change ($\Delta E^* = 42.34$). Crucially, the degradation of lignin destroys its function as a "protective sheath" for cellulose. This exposes the cellulose fibrils to secondary photodegradation, accounting for the observed decrease in both crystallinity and mechanical properties. The impact on mechanical properties was consequently selective: tensile strength, which is highly sensitive to surface flaws like the microcracks observed via SEM (**Fig. 7A**), decreased significantly, whereas compressive strength, a bulk property, was less affected. This highlights a critical diagnostic point: visual surface changes alone may not reflect the bulk structural integrity under non-UV degradation pathways.

Finally, thermal-humidity cycling induced degradation primarily through physical fatigue. Repeated expansion and contraction cycles, driven by temperature and moisture gradients, generated internal mechanical stresses. These stresses led to the fracture and debonding of the wood's microstructure, as visualized

by the prominent cracks in SEM images (Fig. 7B). The significant disruption of the cellulose hydrogen-bond network, evidenced by the reduced -OH peak intensity in the FTIR spectra, confirms a stress-dominated failure mode rather than a chemical one. This finding implies that mitigating physical stresses through environmental control is a key conservation strategy in climates dominated by such cycles.

2. Quantitative Correlations Between Microstructural and Mechanical Degradation

To quantify the relationships between material properties during degradation, Pearson product-moment correlation analysis (Eq. 7) was employed. This analysis provides a robust framework for linking microstructural alterations to changes in mechanical and physical performance.

$$R = \frac{n\sum xy - \sum x \sum y}{\sqrt{\left[n\sum x^2 - \left(\sum x\right)^2\right]\left[n\sum y^2 - \left(\sum y\right)^2\right]}} \quad (7)$$

In this formula, x and y represent the independent and dependent variables, respectively, and n is the number of data pairs in the specific dataset being analyzed. The resulting correlation coefficient, R, ranges from -1 to 1, where an absolute value closer to 1 indicates a stronger linear relationship. The analysis was conducted strictly using the data presented within this study to ensure transparency and reproducibility.

A cross-treatment analysis was first conducted to identify fundamental material properties that govern strength, independent of the specific aging pathway. By correlating the cellulose crystallinity (CrI) from the terminal 30-day aged states and the unaged control (n=4, from Table 6) with the corresponding longitudinal tensile strength (from Table 2), a strong positive correlation was established (R = 0.874). This powerful finding was even more pronounced for compressive (R = 0.902) and bending (R = 0.941) strengths. This identifies Cellulose Crystallinity (CrI) as a key universal predictor of overall mechanical integrity. It underscores the critical role of the crystalline cellulose framework in determining the wood's load-bearing capacity and confirms that its disruption directly leads to strength loss [50]. This finding provides, for the first time, a universal, quantitative link between a microstructural property (CrI) and the residual strength of aged Chinese fir, regardless of the degradation pathway. Its potential for developing a minimally invasive diagnostic tool for in-situ assessment of historic timber members is profound. For instance, a small core sample or even powder drilled from a concealed area could be analyzed by XRD to estimate the load-bearing capacity of a large, irreplaceable beam or column, avoiding destructive testing.

Furthermore, the degradation kinetics within each specific aging protocol were characterized by correlating aging duration with key performance indicators over five time points (n=5). This time-series analysis revealed highly predictable degradation patterns:

For UV weathering, a nearly perfect positive correlation was established between aging time and total color change (ΔE^*) ($R = 0.994$, $p < 0.01$). This demonstrates that surface discoloration is a highly reliable, non-destructive proxy for quantifying the progression of photochemical damage. This validates the use of colorimetry, a completely non-destructive technique, as a reliable proxy for monitoring the extent of UV-induced surface degradation on heritage facades.

For thermal-humidity cycling, aging time exhibited a very strong negative correlation with bending strength (R = -0.963). This highlights the deterministic nature of damage accumulation from physical stresses.

For salt fog exposure, an equally strong negative correlation was found between aging time and compressive strength (R = -0.949), confirming a steady and predictable decline in performance due to chemical degradation.

In summary, these quantitative correlations reveal two key aspects of degradation. First, fundamental properties like tensile strength are intrinsically linked to microstructural features such as cellulose crystallinity. Second, the degradation process under each specific environmental stressor follows a highly predictable, time-dependent trajectory. These strong linear relationships not only deepen the mechanistic understanding of wood aging but also provide a solid quantitative basis for developing service life prediction models.

3. Implications for the Conservation and Management of Timber Heritage

The findings of this study provide a multi-faceted, science-based framework to guide the conservation of timber architectural heritage, bridging fundamental material science with applied practice.

First, the concept of distinct „damage signatures" provides a powerful diagnostic toolkit. By observing specific degradation patterns (e.g., severe surface discoloration versus deep cracking versus chemical erosion, summarized in Table 8), conservators can more accurately diagnose the primary environmental threat affecting a structure. This enables the development of tailored, site-specific intervention strategies rather than generic treatments.

Second, the universal CrI-strength correlation establishes a new paradigm for quantitative structural health assessment. This moves the field beyond traditional

Table 8. Summary of Damage Signatures, Primary Stressors, and Assessment Strategies for Aged Chinese Fir

Observed Signature	Likely Primary Stressor	Assessment and Conservation Recommendations
Severe darkening/discoloration, surface micro-cracking	UV Weathering	Focus on surface protection (e.g., coatings); assess surface tensile properties
Deep cracks/fractures, moderate across-the-board strength loss	Thermal-Humidity Cycling	Prioritize environmental control (stabilize temperature and humidity); assess bulk mechanical properties like bending strength and MOE
Blurred/dissolved cell wall structure, catastrophic and uniform strength loss	Salt Fog Exposure	Conduct chemical analysis (e.g., FTIR) to confirm chemical degradation; use XRD to assess cellulose crystallinity as a proxy for residual core strength

qualitative inspections toward a data-driven approach. The feasibility of using micro-samples for XRD analysis aligns perfectly with the core conservation principle of minimal intervention, offering a practical method for monitoring the safety and stability of historic timber components over time.

Finally, the predictable degradation kinetics offer a quantitative basis for preventive conservation and risk management. By understanding the rate of decay under specific environmental stressors, heritage managers can prioritize interventions, allocate resources more effectively, and develop long-term maintenance plans to mitigate the most significant risks *before* irreversible damage occurs. This proactive, data-informed approach is fundamental to the sustainable preservation of our shared cultural heritage.

Conclusions

Based on this comprehensive investigation, the following primary conclusions are drawn:

1. Chinese fir exhibits distinct "damage signatures" under different environmental stressors, providing a new diagnostic basis for heritage assessment. Salt fog exposure was identified as the most destructive agent, causing severe bulk chemical degradation and a 63.9% loss in bending strength. In contrast, UV weathering was characterized by surface-limited photodegradation, while thermal-humidity cycling caused physically driven damage manifested as a 46.5% strength loss.
2. Cellulose crystallinity (CrI) is a universal predictor of the mechanical integrity of aged Chinese fir, irrespective of the degradation pathway. A strong, treatment-independent linear correlation was established between the reduction in CrI and the loss of tensile (R=0.874), compressive (R=0.902), and bending (R=0.941) strengths. This finding validates the disruption of the crystalline cellulose framework as a fundamental mechanism of degradation and provides a powerful, quantitative basis for minimally invasive structural assessment.
3. The degradation kinetics under specific environmental stressors are highly predictable, enabling quantitative service-life modeling. The decline in mechanical properties for each protocol followed a strong linear trend with aging duration, with most correlations yielding R^2 values greater than 0.87. This predictability, combined with the universal CrI-strength correlation, establishes a robust scientific framework for developing proactive conservation strategies and more accurate service-life prediction models for invaluable timber heritage structures.

Conflict of interest

The author(s) declare(s) that there is no conflict of interest concerning the publication of this article.

Acknowledgements

The research is supported by the Shaanxi Provincial Natural Science Foundation (2025JC-YBMS-560), State Key Laboratory of Tropic Ocean Engineering Materials and Materials Evaluation (STOEM2025KF005), and State Key Laboratory of Safety and Resilience of Civil Engineering in Mountain Area (SQGZ2025118).

References

Hua, Y. W., Chun, Q., & Mi, Z. D. (2023). Experimental research on progressive collapse behavior of Chinese ancient timber buildings with different joint strengthening methods. Journal of Building Engineering, 68, 106215. https://doi.org/10.1016/j.jobe.2023.106215

Li, S., Gao, Y., Brunetti, M., Macchioni, N., Nocetti, M., & Palanti, S. (2019). Mechanical and physical properties of Cunninghamia lanceolata wood decayed by brown rot. iForest – Biogeosciences and Forestry, 12(3), 317–322. https://doi.org/10.3832/ifor2922-012

Da, T. B., & Ha, L. T. N. (2020). A review of Cunninghamia lanceolata (Lamb.) Hook: A recent update and potential application in Vietnam. Vietnam Journal of Agricultural Sciences, 3(4), 892–902. https://doi.org/10.31817/vjas.2020.3.4.12

Zhou, B., Peng, D., Zhao, Q., Yang, S., Yang, F., & Qu, G. (2020). Improvements in timber production of Chinese fir (Cunninghamia lanceolata) per unit forest area in China via tree breeding: Status and challenges. Dendrobiology, 83, 43–51. https://doi.org/10.12657/denbio.083.004

Casagrande, L., Bragante, L., Rosi, A., & Berti, S. (2022). Compressive strength of aged timber members in traditional buildings: Considering differences in heartwood and sapwood. Applied Sciences, 12(15), 7719. https://doi.org/10.3390/app12157719

Feng, J., Cao, Y., Manda, T., Hwarari, D., Chen, J., & Yang, L. (2024). Effects of environmental change scenarios on the potential geographical distribution of Cunninghamia lanceolata (Lamb.) Hook. in China. Forests, 15(5), 830. https://doi.org/10.3390/f15050830

Treu, A., Zimmer, K., Brischke, C., & others. (2019). Durability and protection of timber structures in marine environments in Europe: An overview. BioResources, 14(4), 10161–10184. https://doi.org/10.15376/biores.14.4.Treu

Ebe, K., & Sonoda, T. (2017). Surface deterioration of mixed-type WPC exposed outdoors for promoting weather resistance tests. Journal of Wood Science, 43, 182–195. https://doi.org/10.5990/jwpa.43.182

Grottesi, G., Coelho, G. B. A., & Kraniotis, D. (2023). Heat and moisture induced stress and strain in wooden artefacts and elements in heritage buildings: A review. Applied Sciences, 13(12), 7251. https://doi.org/10.3390/app1312725

Song, X., Gao, T., Ai, M., & Gao, S. (2024). Experimental investigation of tree freeze injury temperatures and their contributing factors based on electrical impedance spectroscopy. Frontiers in Plant Science, 15, 1326038. https://doi.org/10.3389/fpls.2024.1326038

Muhit, I. B., Masia, M. J., & Stewart, M. G. (2023). Failure analysis and structural reliability of unreinforced masonry veneer walls: Influence of wall tie corrosion. Engineering Failure Analysis, 151, 107354. https://doi.org/10.1016/j.engfailanal.2023.107354

Kamath, A., Kumar, G. S. R. K. S., Ravenshorst, G., & van de Kuilen, J.-W. (2025). Mechanical strength characterization of recovered azobé timber boards for reuse. Case Studies in Construction Materials, 22, e04228. https://doi.org/10.1016/j.cscm.2025.e04228

Eslami, H., Jayasinghe, L. B., & Waldmann, D. (2021). Nonlinear three-dimensional anisotropic material model for failure analysis of timber. Engineering Failure Analysis, 130, 105764. https://doi.org/10.1016/j.engfailanal.2021.105764

Caprio, D., & Jockwer, R. (2025). Experimental investigation and probabilistic modelling of the load–displacement behaviour of steel-to-timber joints with self-tapping screws. Construction and Building Materials, 489, 141970. https://doi.org/10.1016/j.conbuildmat.2025.141970

Wang, X., Xu, Q., Wang, X., Guo, J., & Cao, W. (2020). Strength degradation of wood members based on the correlation of natural and accelerated decay experiments. Journal of Renewable Materials, 8(5), 565–577. https://doi.org/10.32604/jrm.2020.09020

Golovin, Y. I., Gusev, A. A., Golovin, D. Y., Matveev, S. M., & Vasyukova, I. A. (2022). Multiscale mechanical performance of wood: From nano- to macro-scale across structure hierarchy and size effects. Nanomaterials, 12(7), 1139. https://doi.org/10.3390/nano12071139

Yang, T., Wang, L., Luo, D., & Mei, C. (2024). Bio-inspired superhydrophobic wood with high stability and durability constructed by using synergies of furfural resin and nano-TiO_2. Construction and Building Materials, 432, 136632. https://doi.org/10.1016/j.conbuildmat.2024.136632

Ferdous, W., & Manalo, A. (2014). Failures of mainline railway sleepers and suggested remedies – Review of current practice. Engineering Failure Analysis, 44, 17–35. https://doi.org/10.1016/j.engfailanal.2014.04.020

Li, M., Wang, L., & Zou, X. (2024). Nondestructive evaluation of carbon fiber reinforced polymer (CFRP)-timber interfacial debonding using active microwave thermography (AMT). Construction and Building Materials, 422, 135786. https://doi.org/10.1016/j.conbuildmat.2024.135786

International Electrotechnical Commission. (2005). Environmental testing – Part 2–30: Tests – Test Db: Damp heat, cyclic (12 h + 12 h cycle) (IEC 60068–2–30:2005). Geneva, Switzerland: IEC.

International Organization for Standardization. (2016). Plastics – Methods of exposure to laboratory light sources – Part 3: Fluorescent UV lamps (ISO 4892–3:2016). Geneva, Switzerland: ISO.

International Organization for Standardization. (2022). Corrosion tests in artificial atmospheres – Salt spray tests (ISO 9227:2022). Geneva, Switzerland: ISO.

Segal, L., Creely, J. J., Martin, A. E., & Conrad, C. M. (1959). An empirical method for estimating the degree of crystallinity of native cellulose using the X-ray diffractometer.

Textile Research Journal, 29(10), 786–794. https://doi.org/10.1177/004051755902901003

International Organization for Standardization. (2014a). Physical and mechanical properties of wood – Test methods for small clear wood specimens – Part 6: Determination of tensile strength parallel to grain (ISO 13061–6:2014). Geneva, Switzerland: ISO.

International Organization for Standardization. (2017). Physical and mechanical properties of wood – Test methods for small clear wood specimens – Part 17: Determination of ultimate stress in compression parallel to grain (ISO 13061–17:2017). Geneva, Switzerland: ISO.

International Organization for Standardization. (2014b). Physical and mechanical properties of wood – Test methods for small clear wood specimens – Part 3: Determination of ultimate strength in static bending (ISO 13061–3:2014). Geneva, Switzerland: ISO.

International Organization for Standardization. (2014c). Physical and mechanical properties of wood – Test methods for small clear wood specimens – Part 4: Determination of modulus of elasticity in static bending (ISO 13061–4:2014). Geneva, Switzerland: ISO.

Batista, N. L., Rezende, M. C., & Botelho, E. C. (2018). Effect of crystallinity on CF/PPS performance under weather exposure: Moisture, salt fog and UV radiation. Polymer Degradation and Stability, 153, 255–261. https://doi.org/10.1016/j.polymdegradstab.2018.03.008

Stadlmann, A., Pramreiter, M., Stingl, R., Kurzböck, C., Jost, T., & Müller, U. (2020). Durability of wood exposed to alternating climate test and natural weathering. Forests, 11(9), 953. https://doi.org/10.3390/f11090953

Nikafshar, S., Nejad, M., Ashrafi, J., & Kord, B. (2022). Evaluating efficacy of different UV-stabilizers/absorbers in reducing UV-degradation of lignin. Holzforschung, 76(3), 235–244. https://doi.org/10.1515/hf-2021-0147

Xu, E., Wang, D., & Lin, L. (2020). Chemical structure and mechanical properties of wood cell walls treated with acid and alkali solution. Forests, 11(1), 87. https://doi.org/10.3390/f11010087

Mo, J., Li, H., & Yuan, J. (2025). Coordination-reinforced lignin/polyvinyl alcohol composites for indoor UV protection and temperature management. International Journal of Biological Macromolecules, 308(Pt 1), 142355. https://doi.org/10.1016/j.ijbiomac.2025.142355

Jakob, M., Mahendran, A. R., Gindl-Altmutter, W., Bliem, P., Konnerth, J., & Müller, U. (2022). The strength and stiffness of oriented wood and cellulose-fibre materials: A review. Progress in Materials Science, 125, 100916. https://doi.org/10.1016/j.pmatsci.2021.100916

Xin, Z., Li, Y., Qiu, X., Zhang, H., Zhou, J., & Yuan, J. (2024). Effects of environmental factors on natural aging of timber members of ancient buildings: Ultraviolet radiation, temperature and moisture. Construction and Building Materials, 456, 139303. https://doi.org/10.1016/j.conbuildmat.2024.139303

Kubojima, Y., Tonosaki, M., & Yoshihara, H. (2023). Aging of wood for musical instruments: Analysis of changes in color, surface morphology, chemical, and physical-acoustical properties during UV and thermal exposure. Polymers, 15(7), 1794. https://doi.org/10.3390/polym15071794

Tang, J., Zhan, T., Li, Z., Jiang, J., & Lyu, J. (2025). Optimization of dimensional stability and mechanical performance of thermally modified wood using cyclic-gradient thermal treatment. Construction and Building Materials, 458, 139596. https://doi.org/10.1016/j.conbuildmat.2024.139596

Mastouri, A., Azadfallah, M., Kamboj, G., Rezaei, F., Tarmian, A., & Efhamisisi, D. (2023). Kinetic studies on photo-degradation of thermally-treated spruce wood during natural weathering: Surface performance, lignin and cellulose crystallinity. Construction and Building Materials, 392, 131923. https://doi.org/10.1016/j.conbuildmat.2023.131923

Sulaiman, N. S., & Mohamad Amini, M. H. (2022). Review on the phase change materials in wood for thermal regulative wood-based products. Forests, 13(10), 1622. https://doi.org/10.3390/f13101622

Idicula, M. K., et al. (2024). Mechanical properties and damage mechanisms of woods under extreme environmental conditions. Case Studies in Construction Materials, 20, e03146. https://doi.org/10.1016/j.cscm.2024.e03146

Gao, S., Zhou, L., Guo, L., Xu, M., & Kang, S. (2022). Mechanical performance degradation of recycled glulam under simulated marine atmosphere. Construction and Building Materials, 346, 128443. https://doi.org/10.1016/j.conbuildmat.2022.128443

Peters, F. B., & Rapp, A. O. (2022). Wavelength-dependent photodegradation of wood and its effects on fluorescence. Holzforschung, 76(1), 60–67. https://doi.org/10.1515/hf-2021-0102

Tintner, J., Smidt, E., Kowarik, K., Grabner, M., & Hinterstoisser, B. (2016). Aging of wood under long-term storage in a salt environment. Wood Science and Technology, 50, 953–961. https://doi.org/10.1007/s00226-016-0830-4

Zhou, L., Gao, S., Xu, M., & Kang, S. (2024). Freeze-thaw effect on performance degradation of recycled glulam from structural members after cyclic loading. Journal of Building Engineering, 72, 109203. https://doi.org/10.1016/j.jobe.2024.109203

Rao, F., Li, X., Li, N., Li, L., Liu, Q., Wang, J., Zhu, X., & Chen, Y. (2022). Photodegradation and photostability of bamboo: Recent advances. ACS Omega, 7(28), 24035–24045. https://doi.org/10.1021/acsomega.2c02035

Cruz-Medina, R., Ayala-Hernández, D. A., Vega-Rios, A., López-Martínez, E. I., Mendoza-Duarte, M. E., Estrada-Monje, A., & Zaragoza-Contreras, E. A. (2021). Curing of cellulose hydrogels by UV radiation

for mechanical reinforcement. Polymers, 13(14), 2342. https://doi.org/10.3390/polym13142342

Zeng, Q., Lai, X., Li, H., Chen, Z., Zeng, X., & Zhang, L. (2024). Wood-based electrolyte with reversible phase transition for smart thermal-shutdown self-protection. Journal of Materials Chemistry A, 12(4), 1642–1653. https://doi.org/10.1039/D3TA06577D

Peng, Y., Fan, Q., Ou, R., Hao, X., Guo, C., & Liu, Z. (2023). Modification of poplar wood cells using 1,3-dihydroxymethyl-4,5-dihydroxyethylideneurea/alkaline lignin for enhanced mechanical properties and decay resistance. Construction and Building Materials, 368, 130354. https://doi.org/10.1016/j.conbuildmat.2023.130354

Haseli, M., Efhamisisi, D., Abdulkhani, A., Oladi, R., Ungerer, B., & Al-Musawi, H. (2024). Effects of oil heat treatment on poplar wood properties: A pilot scale study. Construction and Building Materials, 430, 136353. https://doi.org/10.1016/j.conbuildmat.2024.136353

Laleicke, P. F., & Hubbe, M. A. (2025). Outdoor wood finishing: A review on making wood resistant to moisture, ultraviolet light, and degradation. BioResources, 20(3), Advance online publication. https://doi.org/10.15376/biores.20.3.Laleicke

Csiha, C., Arjona, M. B., Arjona, M. Á., & Ortiz, A. (2021). Study on the mechanical failure of the cellulosic insulation of continuously transposed conductors in power transformers under the influence of short circuits and thermal ageing. Engineering Failure Analysis, 124, 105356. https://doi.org/10.1016/j.engfailanal.2021.105356